THESIS FOR THE DEGREE OF LICENTIATE OF ENGINEERING

Characterizing and Modelling of Surface Roughness and its Impact on Additively Manufactured Fluid Components

ERIKA TUNESKOG

CHALMERS

Department of Industrial and Material Science

CHALMERS UNIVERSITY OF TECHNOLOGY

Gothenburg, Sweden 2024

Characterizing and Modelling of Surface Roughness and its Impact on Additively Manufactured Fluid Components
Erika Tuneskog

Technical report no IMS-2024-15
Department of Industrial and Material Science
Chalmers University of Technology
SE-412 96 Gothenburg
Sweden
Telephone + 46 (0)31-772 1000

Printed by Chalmers Reproservice
Gothenburg, Sweden 2024

ERIKA TUNESKOG
Department of Industrial and Material Science
Chalmers University of Technology

Characterizing and Modelling of Surface Roughness and its Impact on Additively Manufactured Fluid Components

ERIKA TUNESKOG

Department of Industrial and Materials Science
Chalmers University of Technology

Abstract

Reducing emissions in energy production requires adapting gas turbines to renewable fuels, such as hydrogen-based options. However, traditional manufacturing methods limit design flexibility and hinder innovation. Additive manufacturing (AM) techniques, including Powder Bed Fusion Laser Beam (PBF-LB) and Metal Binder Jetting (MBJ), overcome these limitations by enabling high-precision, complex mini-channel designs for gas turbine components. Yet, AM also introduces significant surface roughness, which impacts fluid flow by increasing turbulence and affecting flow dynamics within channels. Accurately predicting pressure loss and heat transfer in these channels is critical to designing effective AM fluid components.

This study examines methods for characterizing AM surfaces, modeling pressure loss and heat transfer, and validating the performance of two demonstrators: a fuel injector and a guide vane, highlighting the unique challenges that surface roughness poses for each component. The fuel injectors were produced from stainless steel 316L using three manufacturing methods: machining, PBF-LB, and MBJ. The guide vane was manufactured with PBF-LB using Inconel 939.

Surface characterization of PBF-LB surfaces for modeling fluid-surface interactions requires multiple roughness metrics. This study proposes that a combination of Sa, Ssk, Spd, Sdr, and S10z provides sufficient surface detail for modeling purposes. Beyond surface roughness characterization, understanding how roughness affects the usable flow-through area is also critical. The study outlines several measurement techniques to address this, including CT scanning for 3D geometry, optical profilometry, and mass flow measurements.

In performance testing, AM-produced fuel injectors were found to be sensitive to surface roughness, with smaller injectors facing manufacturing challenges that resulted in non-circumferential spray patterns. Among the AM injectors, PBF-LB injectors with outlets larger than 0.6 mm demonstrated better spray uniformity and directional stability, despite having higher internal roughness than MBJ injectors. Engine validation tests demonstrated that the advanced cooling design and the favorable internal surface roughness of the AM guide vane channels outperformed those of the cast counterpart, reducing average metal surface temperatures by 56°C and cooling air consumption by 20%.

Keywords: Additive Manufacturing, Hydrogen-rich fuels, Powder Bed Fusion – Laser Beam, Metal Binder Jetting, Surface Roughness, Gas Turbine, Fuel Injectors, Guide vanes

PREFACE

This Licentiate thesis is based on research conducted at the Department of Industrial and Material Science at Chalmers University of Technology from December 2022 to November 2024 and of previous work performed at Siemens Energy published during this period. The work was academically supervised by Professor Lars Nyborg, Senior Lecturer Mats Norell and supported by industry supervision from Dr Karl-Johan Nogenmyr. Professor Emmy Yu Cao was the examiner. This work has been performed within Competence Centre of Technologies and Innovations for a Future Green Hydrogen Economy (TechForH2). The author acknowledges the funding from the Swedish Energy Agency (P2021-90268) and the member companies AB Volvo, Scania CV AB, Siemens Energy AB, GKN Aerospace Sweden AB, PowerCell AB, Oxeon AB, RISE, Stena Rederier AB, Johnson Matthey AB and Insplorion AB.

List of Appended papers

Paper I: **Assessment of Surface Roughness in Additively Manufactured Channels for Fluid Applications**
Erika Tuneskog, Lars Nyborg and Karl-Johan Nogenmyr
EuroPM2024 Conference Proceedings, 2024

Paper II: **Large Eddy Simulations of Flow over Additively Manufactured Surface: Impact of Roughness and Skewness on Turbulent Heat Transfer**
Himani Garg, Guillaume Sahut, Erika Tuneskog, Karl-Johan Nogenmyr and Christer Fureby
Physics of Fluids 36, 085143 (2024). DOI: https://doi.org/10.48550/arXiv.2406.05430

Paper III: **Roughness Related to Cooling Performance of Channels Made Through Additive Manufacturing**
Alexander J. Wildgoose, Karen A. Thole, Erika Tuneskog and Lieke Wang
ASME. Journal of Turbomachinery, Vol. 146, 2024, 051008. DOI: https://doi.org/10.1115/1.4064310

Paper IV: **Exploring Surface Roughness Effects on Spray Performance in Metal Additive Manufactured Spray Nozzles for Gas Turbine Applications**
Erika Tuneskog, Karl-Johan Nogenmyr, Daniel Moëll, Marcus Gullberg and Lars Nyborg
WorldPM2024 Conference Proceedings, 2024

Paper V: **Development and Validation Under Engine Operation Environment of Additively Manufactured Hot Turbine Parts**
Martin Lindbäck, Karin Frankolin, Erika Tuneskog, Björn Karlsson and Lieke Wang
Proceedings of the ASME Turbo Expo 2023. DOI: https://doi.org/10.1115/GT2023-103771

Contribution to the appended papers:
This thesis includes papers from work conducted both during previous employment at Siemens Energy and the current position at Chalmers. The work for Papers II, III and V was carried out at Siemens Energy, but finalized and published after the start of the PhD student position at Chalmers.

Paper I: The author planned and designed the measurements. The surface roughness measurements were performed at RISE. The author conducted the analysis and drafted the paper in cooperation with the co-authors.

Paper II: This is the final article from the CFD4AM project, focusing on CFD simulations of rough surfaces, mainly performed by Ph.D. Himani Garg. The author, along with the co-authors, initiated the project and the author also provided the rough surfaces by co-supervising a master's thesis at Linköping University. The author contributed to drafting the article.

Paper III: The author participated in planning and designing the specimen test matrix based on experience from the SGT800Bx Guide Vane 1. The experiments were performed at Penn State University by Ph.D. Alexander Wildgoose under the supervision of Prof. Karen Thole. The author participated in the interpretation of the results and reviewed the article.

Paper IV: The author collaboratively planned the research with the co-authors and conducted the printing at Chalmers, except for the binder-jetted fuel injectors. The spray measurements were performed at RISE and the author conducted the evaluation and drafted the paper in close cooperation with the co-authors.

Paper V: The author was the responsible heat transfer engineer for the SGT800Bx Guide Vane 1 from the concept phase up to the long-term validation. The author performed all simulation and flow experiments, set the engine test requirements and placed the measurement points for Guide Vane 1. The author evaluated the engine test for SGT800Bx Guide Vane 1 in close collaboration with colleagues.

Table of Contents

NOMENCLATURE

Acronyms

A:	Effective Flow Area / Area of Heat Transfer
D:	Diameter
h:	Convective Heat Transfer
k:	Thermal Conductivity
L:	Length
ṁ:	Mass Flow Rate
Nu:	Nusselt Number
P:	Pressure
Pr:	Prandtl Number
Q:	Heat Transfer per unit of time
Re:	Reynolds Number
T:	Temperature
v:	Velocity

Greek symbols

ρ:	Density
Δ:	Difference
μ:	Dynamic Viscosity

Subscript:

f:	Fluid
s:	Surface
t:	Thickness
h:	Hydraulic

Abbreviations

AM:	Additive Manufacturing
CT:	Computed Tomography
EDM:	Electrical Discharge Machining
HTC:	Heat Transfer Coefficient
LES:	Large Eddy Simulation
LMM:	Lithography-Based Metal Manufacturing
MBJ:	Metal Binder Jetting
PBF-LB:	Powder Bed Fusion – Laser Beam
PDA:	Phase Doppler Anemometry

PSU:	Pennsylvania State University
RISE:	Research Institute of Sweden
SE:	Siemens Energy AB
SEM:	Scanning Electron Microscope
SMD:	Sauter Mean Diameter

1. INTRODUCTION

Reducing emissions in the energy production sector is crucial. This goal places significant demands on the global energy infrastructure, on which many existing solutions rely mainly on fossil fuels, including gas turbines. Despite this, gas turbines have a strong potential to contribute to green energy solutions. Realizing this potential requires the adaptation of gas turbines to use renewable fuels, like hydrogen-rich fuels, with improved efficiency at reasonable costs. Achieving these goals requires advancements in gas turbine components, particularly fluid components. Unfortunately, the limitations of conventional manufacturing methods restrict design freedom, thus limiting performance improvements.

Additive manufacturing (AM) offers an innovative approach to address these challenges. The AM techniques construct 3D objects by layering materials based on digital models [1], which provides greater design freedom than traditional manufacturing methods such as casting. Among AM technologies, only a few are well-suited for producing complex metallic components. Powder Bed Fusion Laser Beam (PBF-LB) and Metal Binder Jetting (MBJ) are preferred due to their ability to produce highly intricate parts with precise tolerances, making them suitable for serial production [2]. In gas turbine applications, components in the turbine and combustion chamber such as guide vanes, heat shields, fuel injectors and burners are especially suited for PBF-LB or MBJ [3]. Many of these components incorporate mini-channels with hydraulic diameters (D_H) ranging from 0.5 mm to 3.0 mm [4]. D_H, is commonly used to determine the equivalent diameter of non-circular channels.

Traditionally, mini-channel designs were limited to straight circular channels. If the channels needed a different shape or were non-straight, the D_H had to be larger than 3 mm. However, AM enables new mini-channel configurations with curved shapes and varying non-circular cross-sections [5]. This capability is a game-changer, allowing designs to be precisely tailored to the specific needs of the component, including efficient wall-integrated designs. However, AM surfaces introduce unique challenges compared to conventionally manufactured surfaces, one of the most important being their inherent surface roughness. The PBF-LB- and MBJ-produced surfaces generally exhibit surface texture, with average surface roughness (Ra) values ranging from 3 to 25 µm, with MBJ surfaces typically falling on the lower end of this range [6]. This becomes impactful in small channels, where performance is sensitive to the characteristics known as relative roughness – the ratio of surface roughness height to D_H [7]–[9]. The PBF-LB and MBJ techniques are both powder-bed-based technologies that create surfaces predominantly characterized by peak-dominated surface textures [10], [11]. In channels smaller than 3 mm (with effects increasing as channel size decreases), these surface peaks can obstruct

the flow, reducing mass flow and increasing friction, which in turn enhances turbulence. Although this turbulence can improve local heat transfer [12], [13], it presents several design challenges.

The relative roughness of additively manufactured channels can be between four to eight times higher than that of conventionally manufactured channels [14], which makes it essential to understand the interaction between surface roughness and fluid flow for effective component design. However, there is limited knowledge of the exact nature of these rough surfaces, including how they can be accurately characterized, modelled and integrated into the design process. Successfully incorporating AM designs into components requires addressing multiple factors. Accurate estimation of AM-produced channel dimensions and surface roughness is crucial; without precise D_H measurements, performance predictions become uncertain. Additionally, surface roughness can vary inconsistently across a component due to variables such as geometry, orientation and the specific printing process. Understanding and managing these variations is critical to achieve reliable and efficient designs.

To address these challenges, it is crucial to understand the fluid interactions with AM-produced rough surfaces, particularly how different types of roughness elements affect fluid flow. This licentiate thesis explores multiple aspects of improving the design of fluid applications with AM. It includes measurements of surface roughness, a combination of simulations with experimental testing of fluid interaction with AM surfaces and component testing, creating a foundational platform for future research in this field. To narrow the scope, the thesis focuses exclusively on as-printed AM surfaces and existing printing parameters. Post-processing methods and the development of new printing parameters as well as further novel sinter-based alternatives will be addressed in later stages of the Ph.D research and is beyond the scope of this licentiate thesis.

1.1. Research Objectives

This study aims to explore the intersection of surface roughness, design for additive manufacturing and fluid mechanics. Target applications included fuel injectors and guide vanes. The objective of the thesis can be summarized through the following research questions (RQ):

RQ1: Which surface roughness metrics best characterize PBF-LB surfaces for fluid applications?

RQ2: How can the usable flow-through area for fluid flow in a PBF-LB- or MBJ-produced channel be measured?

RQ3: How does the internal surface roughness of PBF-LB and MBJ injectors affect circumferential uniformity and spray direction under scaled-down engine conditions in a spray rig?

RQ4: How does surface roughness impact the performance of a PBF-LB-produced guide vane?

2. ADDITIVE MANUFACTURING

Additive manufacturing creates objects layer by layer from digital models, enabling complex and custom geometries by adding material rather than removing it [15]. Among this group of technologies, only a few can produce metal components with high-quality mechanical properties, see Table 1. Directed Energy Deposition (DED) uses focused thermal energy to fuse material as it is deposited, typically resulting in high deposition rates but with rougher surfaces. Lithography-Based Metal Manufacturing (LMM) uses UV light to selectively cure a metal powder-resin mixture, creating high-resolution metal-containing parts which are then debinded and sintered for final density and strength. Metal Binder Jetting (MBJ) involves binding powder particles with a liquid binder before sintering, enabling intricate shapes with minimal post-processing. Powder Bed Fusion Electron Beam (PBF-EB) uses electron beam to melt powder layers, resulting in fast builds with robust thermal management but generally coarser surfaces. Powder Bed Fusion laser beam (PBF-LB) applies a laser beam to fuse powder layers, allowing resolutions and surface finish suited for complex geometries. The DED and PBF-EB are generally unsuited for components requiring high precision owing to their higher energy inputs and larger melt pools, leading to rougher, less detailed finishes. In the case of PBF-EB, the powder bed around the part being built is also slightly sintered to create an inherent support structure, which means that internal channels are difficult to achieve. The LMM has not been available during this licentiate thesis and has therefore been excluded from this work. This thesis has therefore focused on the AM technologies PBF-LB and MBJ.

Table 1: Overview of AM technologies

AM technology	Able to produce mini-channels	Surface roughness below 25µm
DED	**No**	**No**
LMM	**Yes**	**Yes**
MBJ	**Yes**	**Yes**
PBF-EB	**No**	**Possible**
PBF-LB	**Yes**	**Yes**

2.1. Printing Process PBF-LB

The most commonly used metal AM method is PBF-LB [16]. PBF-LB uses a high-powered laser to selectively melt and fuse layers of powder to build three-dimensional objects [17]. This process begins with a thin layer of powder spread across a build platform by the recoater. The laser is then precisely directed according to a digital design to

selectively melt and solidify the powder, layer by layer, creating complex components [18]. In fact, the penetration of the laser beam extends in depth beyond the height of the actual powder. This means that the built material is remelted several times.

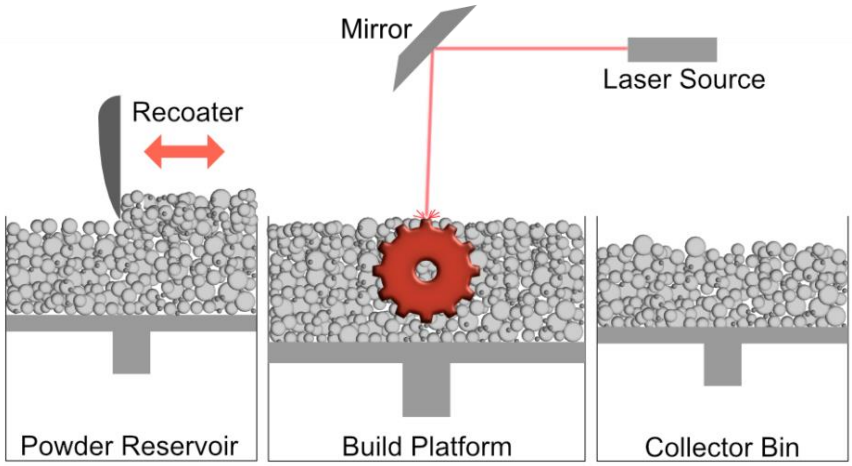

Figure 1: Schematics of a PBF-LB machine.

The PBF-LB components usually have a Sa of 5-25µm attributed to e.g. melt pool dynamics, print orientation and the presence of adhering powder particles and spatter on the surface [19], [20]. Spatter refers to the small particles of metal that are ejected from the melt pool during laser melting,

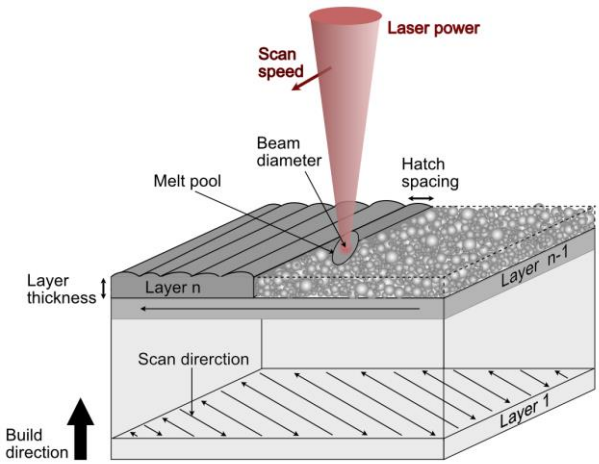

Figure 2: Schematics of printing parameters.

2.2. Printing Process MBJ

The BJM shares similarities with PBF-LB in that both processes utilize a powder bed. However, while PBF-LB employs a laser source to selectively fuse the powder particles, BJM utilizes a liquid binding agent to adhere the particles together [11]. This binding agent is jetted onto the powdered layers according to the desired shape and the process is repeated layer by layer. After the printing process, the excess powder is removed and the component undergoes subsequent debinding and sintering steps to achieve the required mechanical properties and structural integrity [21]. During the process, surface energy acts as the driving force to minimize surface area and reduce total surface energy. Typically, sintering brings the component from a relative density of 60% to 97-99%. Less surface area will result in a more even surface, hence lower surface roughness than for example PBF-LB. However, BJM surfaces still have more texture than conventional manufacturing, especially in form waviness and roughness [22], [23].

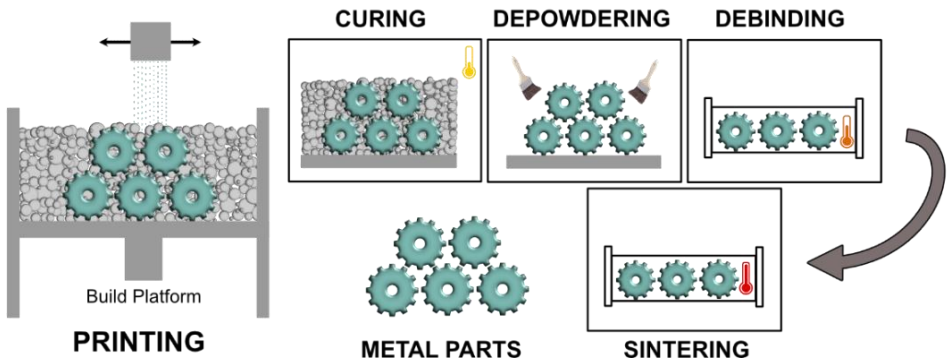

Figure 3: Manufacturing chain for metal BJ.

2.3. Surface Topography

One of the main challenges with AM surfaces is the limited understanding of their surface characteristics. A key issue is the lack of a reliable method to accurately characterize these surfaces. AM surfaces are considerably more textured than conventionally manufactured surfaces such as those that are machined or cast. Due to the manufacturing methods, the surface roughness can be very different in different parts of the component, e.g. vertical vs horizontal (upskin) and 45° surfaces. Consequently, simply measuring Sa or Ra is inadequate for comprehensive surface geometrical characterization, as these metrics do not capture the full complexity of surface topography [24]. This raises the question: how do PBF-LB and MBJ surfaces differ from one another and from conventionally produced surfaces such as machined or cast?

2.3.1. Surface Topography of PBF-LB Surfaces

PBF-LB surfaces can exhibit a wide range of appearances, as shown in Figure 4. One of the most noticeable features is the presence of partially attached powder particles which has sintered on the surface. The degree of attachment varies, with some particles being fully attached to the surface, while others remain connected by only a small contact point. These surface particles typically fall within the original powder particle size distribution, though larger particles can also be present. These larger particles may form from the sintering of several smaller particles or result from spatter from the melt pool, with sizes reaching up to 100µm [20]. The number of particles on the surface can vary significantly, even within the same component, due to factors such as print location, surface orientation, laser incident angle, process parameters and geometry. Beneath the particle layer, the surface exhibits a textured appearance characterized by general waviness. This waviness varies across different surfaces and can be significantly influenced by process parameters. The causes of this waviness may include the layer-by-layer construction process, the staircase effect and factors like hatch distance, such as the overlap and thickness of the melt pool in PBF-LB.

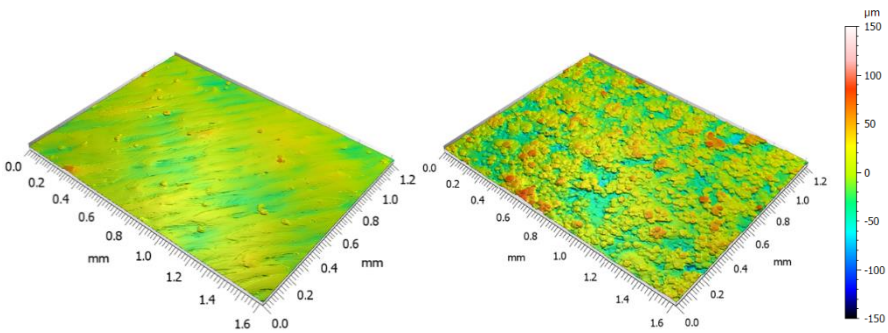

Figure 4: Variation of PBF-LB printed surfaces [25].

2.3.2. Surface Topography of MBJ Surfaces

The MBJ surfaces exhibit similar characteristics to PBF-LB surfaces, with partially sintered powder particles from the powder bed process. However, the appearance of attached particles differs because MBJ surfaces are sintered. The attachment area between the surface and powder particles is generally larger than on PBF-LB surfaces, see Figure 5. Like PBF-LB surfaces, MBJ surfaces also display a textured appearance with a general waviness [26], [27]. This effect can be explained by the binder droplet wetting and penetrating the powder; the binder's surface tension often causes powder balling and rearrangement of particles within the primitive, resulting in visible lines across the surface [28].

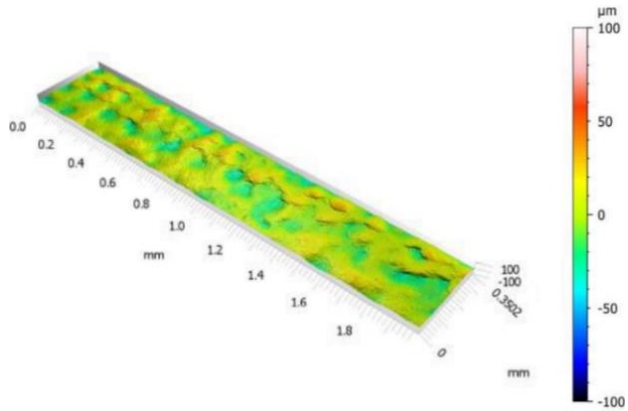

Figure 5: MBJ surface topography [29].

3. FLUID SURFACE INTERACTION

There is currently a lack of precise estimations of the performance of AM-fabricated components [30]. To illustrate, if we assume the surface roughness height is approximately the same as the maximum powder particle size for PBF-LB or MBJ in a 1.0 mm channel, the relative roughness would be about 10% and 5% of the channel diameter, respectively. In comparison, conventional computational fluid dynamics (CFD) software can generally predict fluid flow accurately when relative roughness is within a 2-3% range. However, both PBF-LB and MBJ-produced channels often exceed this range, leading to challenges in modelling. This raises the question: Why is fluid behavior significantly different in rough channels?

3.1. Fluid Flow in Rough Channels

Fluid flow in rough channels exhibits different fluid behavior compared to smooth channels due to surface roughness elements that create a blockage effect, also known as drag. In the fully rough regime, peak-dominated surfaces exhibit higher friction due to intensified turbulence and drag [14]. The skin friction concentrates at the front of protrusions due to flow separation and recirculation, while in cavity-dominated surfaces, reattachment occurs further downstream, boosting turbulence and momentum transfer [12], [13]. Roughness impacts heat transfer by increasing near-wall turbulence, with upstream peaks enhancing fluid mixing and convective heat transfer. Similarly, normalized Nusselt number Nu/Nu_0 (effectiveness of thermal energy transfer) rises with roughness, showing significant heat transfer enhancement in the fully rough regime, where peak-dominated surfaces outperform valley-dominated ones, indicating that roughness disrupts the thermal boundary layer and enhances heat transfer [31], [32].

Studies on channels ~1 mm indicate that the pressure loss in AM-produced mini-channels can be three to four times greater than that in conventionally manufactured channels due to the rough surfaces [32]–[34].

3.1.1. Friction Factor and Heat Transfer Coefficient (HTC)

The Darcy friction factor, commonly used to represent pressure losses in channels, is defined as:

$$f = \frac{\Delta p \cdot dh}{L \cdot \rho \cdot u^2/2} \qquad \text{Eq. 1}$$

where Δp is the pressure difference, dh the hydraulic diameter, L the channel length, ρ the fluid density and u the flow velocity. More details regarding the naming can be found in the Nomenclature section. Results are typically plotted in a Moody diagram, comparing with theoretical predictions for fully developed laminar flow f=64/Re and the White-Colebrook equation [35] for turbulent flow, which considers Reynolds number and relative roughness, k_s/D_H [36], see Equation 2.

$$\frac{1}{\sqrt{f_d}} = -2.0 \log_{10}\left(\frac{k_s/D_H}{3.7} + \frac{2.51}{Re\sqrt{f_d}}\right) \qquad \text{Eq. 2}$$

From the earliest experiments of surface roughness influence in pipe flow, sand was used to create the wall roughness, therefore sand grain height (diameter) (k_s) is defined as a layer of closely packed spheres, see Figure 6 [9]. However, sand grain height is not very useful in industrial applications, leading to the concept of equivalent sand grain roughness, which establishes a relationship between sand grain roughness and various rough surfaces [9]. This measure is typically determined through experimental methods and applies across a wide range of fluid applications [37]. Currently, there is no universally accepted equivalent sand grain roughness for AM mini-channels but there is a lot of ongoing research to develop correlations [14], [33], [38]–[42]. The limited experimental dataset and the variation in surface roughness complicate efforts to create a coherent correlation that accurately matches all available data.

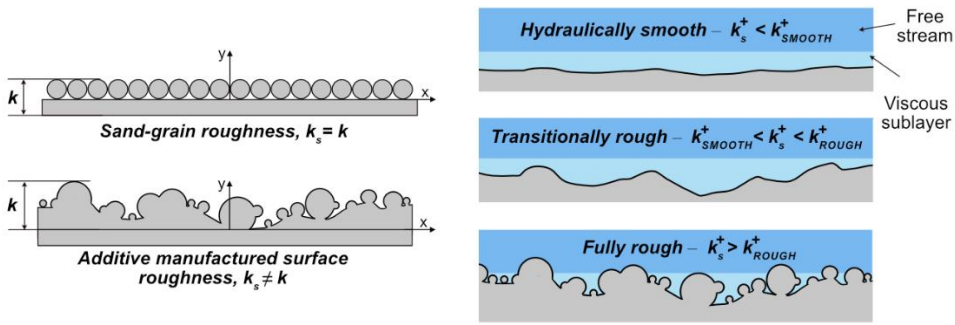

Figure 6: Illustration of sand grain roughness in an AM context (illustration adapted from [24], [31]).

The Gnielinski correlation is an empirical formula used for calculating the Nusselt number (Nu) for turbulent flow in pipes, particularly for fully developed flow. The Nusselt number represents the non-dimensional heat transfer rate, assuming an axisymmetric temperature distribution in circular channels. To predict air outlet temperature, the flow direction is discretized, and local air and wall temperatures are calculated, which then are compared to experimental measurements under various heating conditions, see Equation 3. The Gnielinski equation incorporates both the Reynolds number and the Prandtl number, as

these two parameters account for the key factors influencing convective heat transfer: The flow characteristics of the fluid (Re) and its thermal properties (Pr), as follows.

$$Nu = \frac{f_d/8\,(Re_D - 1000)Pr}{1 + 12.7\sqrt{f_d/8}\left(Pr^{\frac{2}{3}} - 1\right)} \qquad \text{Eq. 3}$$

3.2. Hydraulic Diameter

D_H is a calculated value used to characterize non-circular ducts or channels in fluid flow, defined as four times the cross-sectional flow area divided by the wetted perimeter. Defining D_H in AM-produced channels is surprisingly complex. The large surface roughness makes it hard to determine the cross-section area. For smoother channels, D_H can be accurately calculated from CAD models, but this method is unsuitable for channels with large relative roughness. Roughness can reduce the effective D_H of AM mini-channels by up to 10% [43]. Three alternative methods can provide better D_H estimations. The first approach involves visually examining the channel output using an optical microscope, manually outline the perimeter and subsequently calculate the hydraulic diameter based on these observations [33], [40]. Because of the manual work and user-dependent evaluation of the cross-section, there are uncertainties in the result. The second approach also focuses on the channel cross-sections but employs external Computed Tomography (CT) scanning to measure multiple cross-sections and estimate an average channel diameter [32], [38], [39], [44], [45]. However, this method has limitations, especially in its inability to capture all surface details accurately. The last approach relies on flow measurements, using mass flow, pressure loss and temperature data to calculate the cross-sectional area [46].

3.3. Surface Roughness Parameters for Fluid Applications

In fluid applications, a crucial aspect of evaluating surface roughness is accurately defining surface peaks, as these significantly impact fluid flow behavior [13]. Key characteristics include the height difference between valleys and peaks, as well as deviations from the surface's arithmetic mean. The shape of the topography, whether dominated by peaks or valleys, also plays a critical role. Additionally, the texture and specific properties of the peaks, such as their height, density and distribution per unit area, influence flow dynamics. These factors are essential for understanding how surface roughness affects the flow resistance and performance in fluid systems and can be summarized as follows.

- **Sa (Arithmetical Mean Height):** The absolute height deviations from the arithmetical mean of the surface (ISO 25178).

$$S_a = \frac{1}{A} \iint_A |Z(x,y)| dx\, dy \qquad \text{Eq. 4}$$

- **S10z (Ten-point height):** Height above the mean surface for the five highest local maxima and the height below the mean surface for the five lowest local minima (ISO 25178).

- **Ssk (Skewness):** Roughness shape (asperity) measures whether the surface is peak- or valley-dominated (ISO 25178).

$$S_{sk} = \frac{1}{Sq^3}\left[\frac{1}{A} \iint_A |Z^3(x,y)| dx\, dy\right] \qquad \text{Eq. 5}$$

- **Sdr (Developed Interfacial Area Ratio):** Percentage of the definition area's additional surface area contributed by the texture as compared to the planar definition area (ISO 25178).

$$S_{dr} = \frac{1}{A}\left[\iint_A \left(\sqrt{\left[1 + \left(\frac{\partial z(x,y)}{\partial x}\right)^2 + \left(\frac{\partial z(x,y)}{\partial y}\right)^2\right]} - 1\right) dx\, dy\right] \qquad \text{Eq. 6}$$

- **Spd (Density of peaks):** Representation of number of peaks per unit area (ISO 25178).

4. GAS TURBINE COMPONENTS

A gas turbine is an engine that generates power by burning fuel to produce high-temperature, high-pressure gases. These gases drive turbine blades connected to a rotating shaft, which can produce electricity, power aircrafts, or drive machinery. It has three main sections: a compressor to pressurize air, a combustion chamber to burn fuel and a turbine to convert hot gas energy into rotational force. Gas turbines are highly efficient and widely used in power generation and aviation.

4.1. Guide Vane

In the turbine section of a gas turbine, guide vanes are stationary blades that direct high-velocity gas from the combustion chamber towards the turbine rotor blades. These vanes control the angle and speed of the gas, maximizing energy transfer and turbine efficiency by ensuring optimal impact on the rotating blades. Operating in extreme environments with temperatures over 1000°C, guide vanes are made of nickel-based superalloys and in early stages, include cooling channels and thermal barrier coatings to reduce metal temperature and extend lifespan.

To improve turbine efficiency, temperatures need to be maximized, yet cooling must be carefully managed, as this lowers temperature and diverts air from enhancing efficiency. Although cooling reduces overall efficiency, it is necessary for component durability in such harsh environments. AM is promising here, as its cooling designs have been shown to lower component temperatures, reduce thermal gradients and conserve coolant [46]. AM-produced channels can also be much smaller than cast ones, sometimes reaching functional diameters below 0.8 mm [47].

4.2. Fuel Injector

The fuel injector delivers and atomizes fuel into the combustion chamber, where it is mixed with compressed air for efficient ignition and combustion. Positioned within the combustor, injectors create a fine fuel mist, improve air-fuel mixing, combustion stability and efficiency while minimizing emissions. Precise fuel delivery is critical for consistent power output and efficient turbine performance [48].

In the future, gas turbines will need to transition away from fossil fuels. Hydrogen-rich fuels are strong candidates for low-emission energy production, but this shift brings challenges for fuel injectors, which will need enhanced fuel flexibility and optimized

injection for diverse fuel types. AM offers the design freedom to develop such advanced injectors. However, the textured AM surfaces near the orifice exit can lead to problems, including reduced spray uniformity and larger spray droplet sizes. These effects stem from higher friction loss, which reduces the energy available for fuel breakup, impacting overall combustion efficiency [49]–[51].

5. METHODOLOGY

When designing fluid components with AM, many uncertainties arise throughout the process due to limited knowledge in AM-based component development. In earlier chapters, we explored challenges related to surface roughness; here, the impact of these factors on component development is examined, following these steps:

1. Set process and print parameters for specific material (outside of scope).
2. Develop methods to predict friction factors and HTC for the specific material.
3. Design a component concept and apply developed correlations.
4. Iterate component design with prototype prints and prototype tests.
    a. Measure D_H considering the influence of both shrinkage and surface roughness.
    b. Verify component design.
5. Evaluate component performance.

5.1. Development of Methods to Predict Friction Factor and HTC

An experimental dataset for a specific material requires a test rig to measure friction factors and bulk convection coefficients across transitional and fully turbulent flows. Friction factors are calculated using the pressure drop across a test coupon, with mass flow rate regulated upstream through a laminar flow element and backpressure adjustments downstream to ensure fully turbulent flow. The D_H of the channel and flow rate data are incorporated into the friction factor calculation, while an inlet loss coefficient is derived from the area ratio between the plenum and sample inlet. For convection measurements, heaters keep a constant surface temperature on each side of the coupon, while thermocouples measure internal channel temperatures through a conduction model [38].

5.2. Materials and Manufacturing Process

As shown in Table 2, few constants exist across the various studies; materials, powders, manufacturing methods, printers and print parameters all differ. Therefore, only a general overview of the component and test specimen production methods is provided. For all PBF-LB samples and components fabricated, print parameters were selected based on best-practice experience at the time of printing at Chalmers and Siemens Energy (SE). Printer selection was based on site availability. The MBJ printed components were provided by RISE and Markforged and sintered by RISE in a graphite furnace at 1310°C using a low-pressure argon as the protective gas to reach approximately 98% density. As indicated in

the table, three materials were used: Stainless Steel 316L, Inconel 939 and STAL15DE [52]. Inconel 939 and STAL15DE were chosen for the guide vane due to high-temperature requirements, while Stainless Steel 316L was used for the fuel injector. Only 316L was processed using either PBF-B or MBJ. Table 2 summarizes the materials and manufacturing methods applied.

Table 2: Overview of material and manufacturing

Material	**Powder Particle Size Distribution**	**AM Method**	**Layer Thickness**	**Printer**	**Paper**
Stainless Steel 316L	20-53µm	PBF-LB	20µm	EOS M290 *(Chalmers)*	I
Inconel 939	15-45µm	PBF-LB	40µm	EOS M400-4 (*SE AB*)	II
STAL15DE	15-45µm	PBF-LB	40µm	EOS M400-4 (*SE AB*)	III
Stainless Steel 316L	20-53µm, 5-20µm	PBF-LB, MBJ	20µm	EOS M100 *(Chalmers)* Markforged DMP2500 (*RISE and Markforged*)	IV
Inconel 939	15-45µm	PBF-LB	40µm	EOS M400-4 (*SE AB*)	V

For post-printing steps, similar precautions were taken to avoid surface damage. In Papers I–III, samples were cut directly from the build plate and sent for surface roughness measurements without any additional post-processing. In contrast, the components in Papers IV–V underwent further post-processing, including machining for support removal, as well as heat treatments and shot peening (Paper V). However, no additional post-processing was performed on any of the internal channels.

5.3. Surface Roughness and D_H Measurements

Various methods have been used to evaluate surface roughness and D_H across studies, as summarized in Table 3. These assessments, covering both flat and curved surfaces with

contact and non-contact techniques, aim to understand how surface roughness in internal channels affects D_H.

In this thesis, two different optical methods: confocal fusion microscopy (Paper I) and focus variation microscopy (Paper II) were utilized to measure surface roughness. Surface roughness was analyzed by capturing images at different focal planes. As the objective moves along the z-axis, the in-focus areas correspond to specific heights, which are then combined to form a complete representation of the surface. The resulting data can be refined with filters, such as high-pass or Gaussian, to remove artifacts. The measuring point density achieved with focus variation is lower than that of confocal microscopy due to its lower resolution. High-reflective, low-contrast surfaces, in particular, present physical limitations for focus variation.

Surface roughness measurements for Paper I were conducted at RISE, while those for Paper II were performed by master's student Sebastian Richter at Linköping University under the supervision of Erika Tuneskog and Karl-Johan Nogenmyr [53].

Computed tomography (CT) scanning was used in Paper III [14] as a nondestructive method to evaluate internal channel geometry, detect blockages and calculate the hydraulic diameter (D_H). Scans at a 35-micron voxel resolution provided grayscale data, allowing for the calculation of D_H, cross-sectional area and perimeter by averaging streamwise slices. Key metrics: concentricity, circularity and total runout, were derived by transforming perimeter data into a 3D point cloud. Concentricity measures centroid alignment, circularity indicates shape accuracy and total runout combines both to assess straightness. Surface details were interpolated to one-tenth voxel size, enabling precise geometric analysis [30].

In Papers IV and V, D_H measurements were initially conducted by outlining the channel perimeter from images of the channel cross-section or outlets using optical measurements. However, these measurements proved to be unreliable, so experimental mass flow data also known as cold flow tests was instead used for calculating cross-section area, see Equation 7, A is the required cross-sectional area to accommodate a certain mass flow rate $\dot{m}$, given the density of the fluid ρ and the pressure difference ΔP.

$$A = \frac{\dot{m}}{\sqrt{2\rho\Delta P}} \qquad \text{Eq. 7}$$

Table 3: Surface roughness and D_H measurements

Paper	Type of Measurement	Equipment
I	Optical Measurement – Flat Surfaces	SensoFar Neox S
II	Optical Measurements – Flat Surfaces	Leica DM6 M
III	Computer Tomography – Channels System	Equipment PSU
IV	Optical Measurement – Half Channels, Outlets Mass Flow Measurements – Full Component	SensoFar Neox S Spray Rig RISE
V	Optical Measurement – Cross-Section Channels Mass Flow Measurements – Full Component	Equipment SE Cold Flow Rig SE

5.4. Components

For this thesis study, two different AM components have been used as reference and demonstrator objects as described below.

5.4.1. Fuel Injector (Paper IV)

This study examines how surface roughness from two AM processes affects spray performance and evaluates the feasibility of using AM fuel injectors without post-processing. To minimize design effects, a simple orifice design was selected, with a single outlet comprising two connected segments and a filler in between, see Figure 7. The larger segment has twice the diameter of the smaller one and the length-to-diameter (L/d) ratio for each segment follows Lefebvre's [48] recommendation of four. Twenty-six 316L stainless steel fuel injectors were fabricated for testing, divided into seven groups with outlet sizes of 0.5 mm, 0.6 mm, 0.7 mm and 1.0 mm, produced using PBF-LB and MBJ methods.

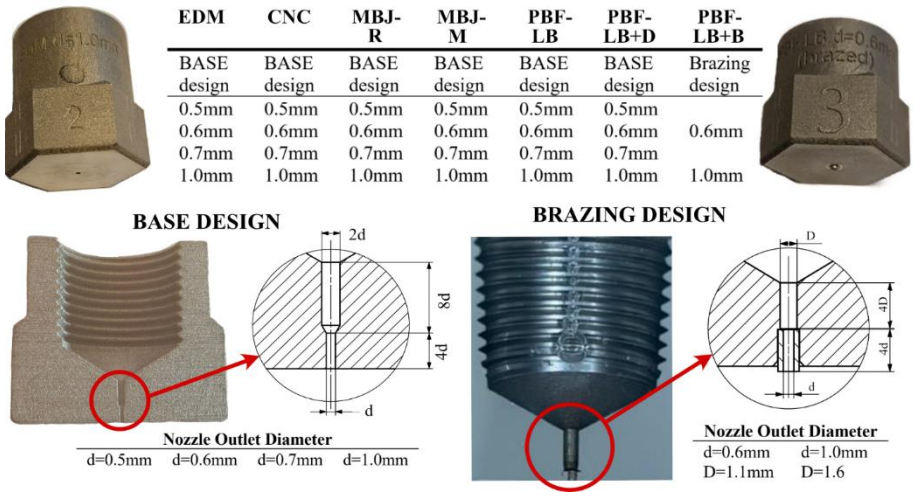

Figure 7: Design of fuel injectors with test matrix.

The spray rig at the RISE Energy Technology Centre in Piteå was used for experimental simulation. Although measurements are done at room temperature, the test conditions are set to capture the potential flow characteristics in real applications. This rig facilitated high-speed photography of fuel injector spray patterns. Pressurized with compressed air and nitrogen, the rig featured four optical windows (0°, 90°, 150°, -106.3°) for multi-angle imaging [54]. Water was used as the test liquid and tests were conducted at 8.5 bar rig pressure and 61.7 bar fuel pressure to simulate scaled-down cold gas turbine conditions. Measurements included fuel pressure, vessel pressure, mass flow and temperature. Each injector test captured 250 images per position, totaling 750 images at 0°, 45° and 90° angles.

The image quality and frame rate were sufficient to assess spray shape, including uniformity, angle and direction, but inadequate for detailed analyses of droplet shape, size, or velocity due to low resolution. The images were processed in MATLAB R2023b by converting images to binary to isolate the spray core. The largest coherent spray structure was identified. Spray width was calculated by counting pixel columns between boundaries and spray angle was determined by fitting polynomial trendlines to the edges, as shown in Figure 8. These metrics were then averaged across angles to evaluate spray characteristics.

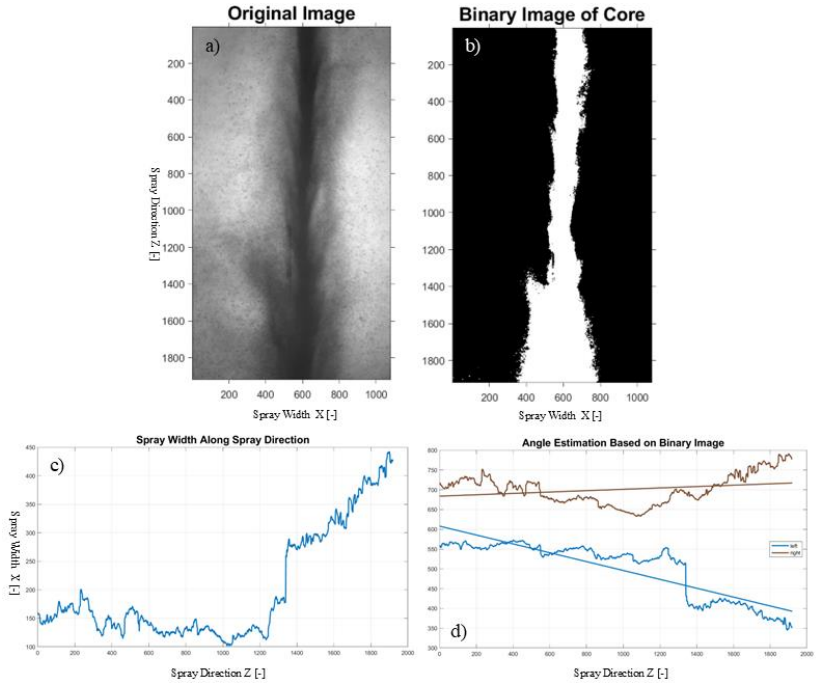

Figure 8: Image processing steps of spray.

A secondary, more extensive test using the Phase Doppler Anemometry (PDA) technique was performed on three fuel injectors: MBJ-R 0.7mm, PBF-LB 0.6mm, and PBF-Brazed 0.6mm. PDA measures particle velocity and size by utilizing the principles of light scattering by spherical particles. This method relies on the interference of two laser beams or scattered waves within the measurement volume, creating a fringe pattern. The velocity of moving scattering centers is derived from the Doppler effect in the scattered field. The setup is mounted on a precision-controlled traverse table, enabling comprehensive spray measurements. For each measurement point, two criteria are established: either 10,000 droplets are captured, or 30 seconds have passed. Once one of these criteria is met, the PDA system advances to the next measurement point. The measurements were performed on two planes 95 mm and 142 mm and in a cross pattern as illustrated in Figure 9.

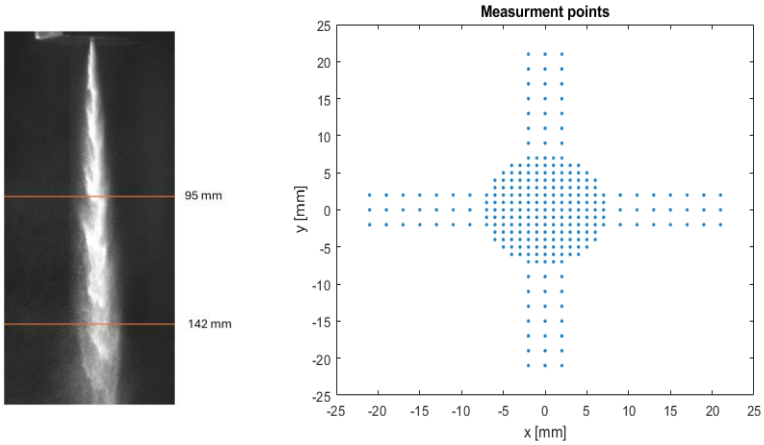

Figure 9: (a). Location of measurement plane. (b). Placement of the 261 measurement points for PDA.

5.4.2. Guide Vane (Paper V)

The design process leading up to the final design was iterative, involving the continuous refinement of the design model by integrating requirements for aerodynamics, material, mechanical integrity, heat transfer and cost. The overall cooling design consisted of embedded mini-channels within the vane walls, allowing for thinner walls and thus less material to cool and for more surface area between rough walls and fluid, to yield a more efficient cooling scheme. The design also eliminated the need for additional inserts, as shown in Figure 10. Once the design model was finished a prototype was printed and subjected to various minor tests, including cold flow (mass flow) measurements, thermal imaging, water tests, microstructure analysis, etc. Based on the results of these tests, the design model was adjusted to address any identified issues.

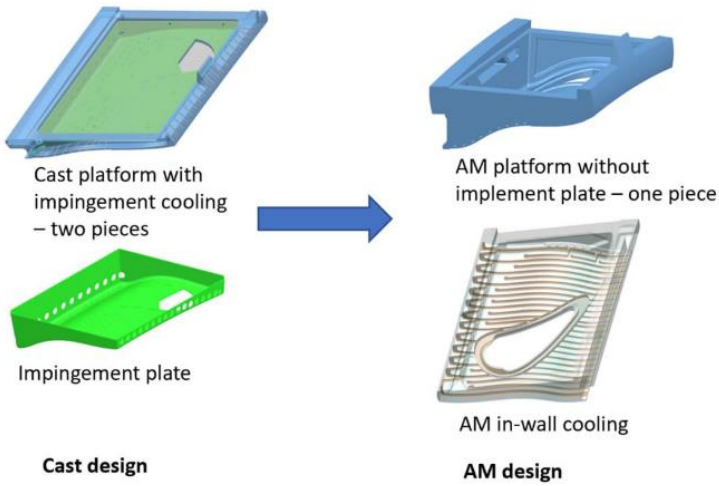

Figure 10: Comparison of cast vs AM design [46].

A large-scale engine test validated the AM design, with components instrumented using thermocouples and silicon carbide thermo-crystals to measure surface temperature. The crystals, exposed to neutron scatter radiation, develop crystal defects that expand the lattice. When heated, the crystals attempt to revert to their original state and the resulting scattering angle can indicate temperature if the exposure duration is known. Thermocouples provided in-situ temperature readings to support the crystal data. The crystals offer high precision, with ±15°C accuracy at 1000°C.

6. SUMMARY OF APPENDED PAPERS

As mentioned earlier, surface roughness is one of the main challenges for fluid components produced by AM. One of our first steps must be to characterize these surfaces to accurately describe them. If we start with characterization, which surface roughness characteristics would be relevant to describe?

6.1. Surface Roughness Characterization of AM Surfaces

Paper I examines various flat PBF-LB surfaces to determine how their characteristics can be accurately described using surface roughness parameters, with a focus on areal parameters for enhanced accuracy. While Sa values indicate roughness levels, they are insufficient for fully characterizing surface texture. Instead, the study highlights the importance of S_{SK} (skewness) as a key parameter for distinguishing between peak- and valley-dominated surfaces. It identifies two primary issues associated with non-peak-dominated surfaces: a high density of partly sintered particles covering the surface and insufficient energy density, which results in gaps between melt pools. When combined with S_{PD} (Peak Density), S10z (Maximum Height of Peaks) and S_{DR} (Relative Surface Area), the underlying causes can be identified.

Still, there are limitations to using non-contact methods like optical measurements, such as shading effects that distort data capture and difficulties in measuring curved surfaces. Another alternative used in Paper III is CT of full channels, which can effectively capture shaded surfaces but is limited by a resolution of approximately 5 µm.

There is thus an overall challenge, as neither FVM nor CT can fully assess the internal surface roughness of the channels. The detailed level of AM surfaces required for simulation work in CFD could not be achieved from any channel measurements. Therefore, for Paper II, a flat 1.0 mm x 1.0 mm surface was measured with FVM and numerically transposed to represent a circular channel.

6.2. Modelling of Rough Channels

In Papers II and III, two approaches are outlined for understanding and modelling the influence of surface roughness in pipe flows: simulation using CFD and experimental correlations. A key challenge is understanding the interactions between the fluid and the channel walls. This interaction can be studied through various experimental and simulation

methods, each providing unique insights. However, surface roughness presents notable limitations. Current CFD simulations for heat transfer and pressure loss in mini-channels often lack accuracy and fail to provide reliable predictions. To overcome these challenges, there is a need to develop roughness models within CFD that can effectively address the unique surface roughness characteristics found in AM mini-channels. Achieving this goal requires identifying the most relevant AM roughness parameters for modelling. Additionally, understanding how factors such as powder particle size distribution, the presence of partially attached powder particles, waviness and surface height influence fluid flow is essential for improving simulation accuracy.

The study performed in Paper II is the first step towards gaining deeper understanding of the interaction between rough surfaces and fluid flow. In Paper III, the focus is on the correlations made for component development. These correlations have been used in component development with good results.

6.3. Channel Dimension

To design components with the desired mass flow, heat transfer and pressure loss, it is essential to estimate the usable flow-through area of the channels. However, as described in the methodology section, there are multiple ways to estimate this area and no single approach guarantees the most accurate results. Two methods, optical measurements and CT, are described in Papers III-V. Both start by estimating the surface perimeter of a single-channel cross-section. optical measurements limitation is that it typically examines only a few cross-sections, potentially overlooking surface defects that could reduce the actual flow-through area, leading to an overestimation. For CT, the main issue is channel resolution; since scanning is done without opening the channels and must penetrate the sample wall, resolution is reduced, resulting in artificially smoother surfaces.

To address these limitations, measuring the mass flow through the component is often a simpler approach. If a model accounts for friction losses, it becomes relatively straightforward to calculate the minimum flow-through area of a flow group or the entire component.

6.4. Components

Two different demonstrator components, the fuel injector and the guide vane, were printed and evaluated. The fuel injector was printed without adjustments for surface roughness or potential shrinkage, while the guide vane dimension correction factors were applied to achieve cross-sections that support specific mass flow.

6.4.1. Fuel Injector

In the study presented in Paper IV, twelve fuel injectors were printed with outlet sizes ranging from 0.5 mm to 1.0 mm to account for reduced mass flow and flow-through areas owing to surface roughness and shrinkage, especially in smaller outlets, which is influenced by relative roughness. The smallest injectors, with minimum outlet sizes of 0.5 mm to 0.6 mm, showed the largest flow-through area reduction of 40–65%, caused by a combination of shrinkage and surface roughness. These injectors did not perform well and exhibited poor circumferential uniformity and inconsistent spray patterns, as shown in Figure 11, where the average profiles of the two smallest injectors (first column) do not overlap. Surprisingly, MBJ injectors generally performed worse than PBF-LB injectors, despite PBF-LB surfaces typically being rougher with higher surfaces peaks and more surface texture. The reasons for this outcome are not fully understood and further roughness measurements with CT are required. In summary, PBF-LB injectors showed the best uniformity in larger outlets.

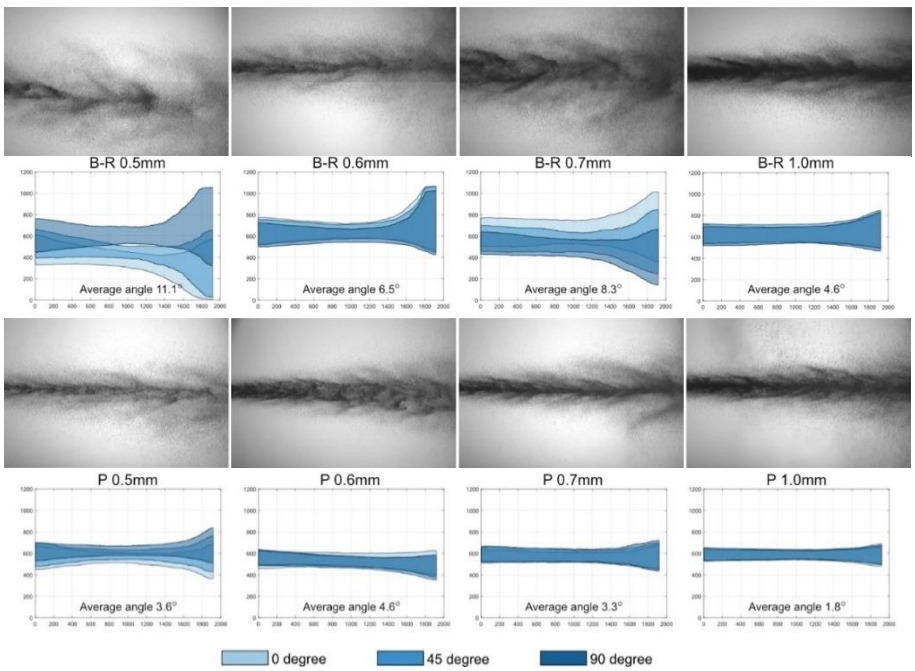

Figure 11: Spray cone MBJ injectors (first two rows) and PBF-LB injectors (last two rows). Each column represents one size of a fuel injector. The first and third rows display examples of spray behavior and the second and fourth rows provide an average spray shape for each fuel injector.

From the selection above, the MBJ 0.7 mm and PBF-LB 0.6 mm injectors were chosen for more extensive PDA testing based on their mass flows. The results show differences in

velocity between the two injectors, with the spray from the PBF injector not breaking apart as much and maintaining a more defined spray core with a higher velocity see Figure 12. The highest average velocities for PBF and MBJ were 37 m/s and 28 m/s, respectively. The difference in spray break-up characteristics did not significantly affect the Sauter Mean Diameter (SMD) of the injectors, although droplet size decreased from approximately 125 µm to 104 µm as the distance from the injector outlet increased see Figure 13.

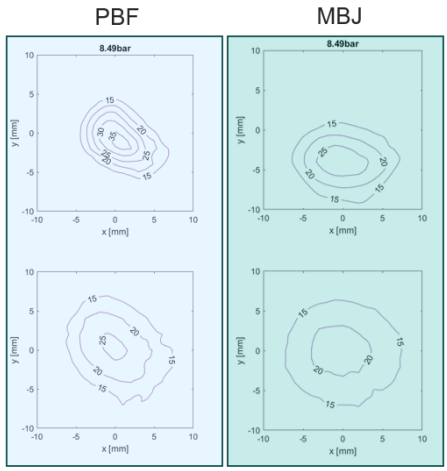

Figure 12: The velocity profile for the three PDA-tested injectors at a pressure ratio of 53.20 bar with diesel fuel is shown, with measurements taken at 95 mm (upper row) and 142 mm (lower row) from the injector outlet.

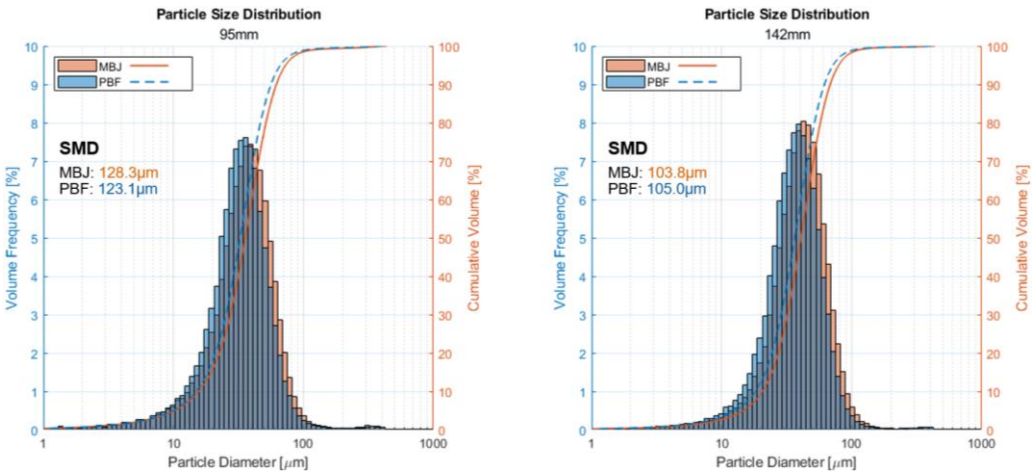

Figure 13: The particle diameter distribution for the three PDA-tested injectors at a pressure ratio of 53.20 bar with diesel fuel is shown.

6.4.2. Guide Vane

This summary is based on Paper V, which details the component's development through several print iterations and various performance evaluation tests, including mass flow and heat transfer measurements. In the initial iterations, the channel cross-sectional area was reduced by over 20%, depending on factors such as location, channel orientation and design aspects that influenced the printing parameters.

While the specific friction factor and heat transfer coefficient used in the analysis have not been published, they are derived from experiments, similar to those in Paper III, but specifically for Inconel 939. These correlations were applied to model the pressure loss and heat transfer of the guide vane. The model of the AM guide vane required only minor adjustments to align with the measured temperatures from the validation tests.

Engine validation results showed that the AM components achieved a significant reduction in metal surface temperatures, decreasing by 56°C, along with a 20% reduction in cooling air consumption compared to their cast counterparts. This success is attributed to advancements in the cooling scheme design and the benefits provided by the internal surface roughness of the cooling channels. Additionally, the reduction in hot spots and temperature gradients resulted in a lower thermal load on the components, as illustrated in Figure 14. Several problematic hot spots were either eliminated completely or significantly reduced in severity. In conclusion, modelling AM-developed correlations for the friction factor and heat transfer coefficient proves to be an effective approach for designing AM components that outperform conventional alternatives.

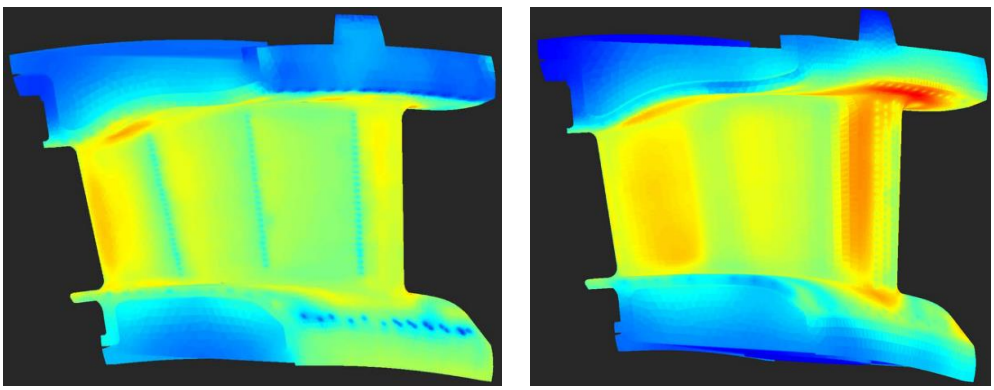

Figure 14: a). Normalized temperature of AM GV1. b). Normalized temperature of cast GV1 [46].

7. CONCLUSIONS

Based on the results provided in this thesis study the following conclusions can be made in relation to the research questions raised.

RQ1: Which surface roughness metrics best characterize PBF-LB surfaces for fluid applications?

- Paper I asserts that using Sa alone is insufficient to characterize AM surfaces.
- Incorporating additional parameters like Ssk, Spd, Sdr and S10z provides a more holistic understanding of surface textures.
- Further research is needed to refine these metrics and develop improved methods for analyzing surface roughness on complex geometries, particularly to distinguish between sizes of partly sintered particles and spatter.

RQ2: How can the usable flow-through area for fluid flow in a PBF-LB or MBJ-produced channel be measured?

- CT scanning provides detailed 3D images of internal channel geometries. This Allows the measurement of flow-through area by capturing channel surfaces. Important is to consider scanning resolution, as lower resolutions can result in inaccuracies for rough surfaces.
- Optical measurements offer high-resolution surface measurements to assess surface roughness, which is crucial for determining effective flow area. The technique can capture geometric features of channels, but requires line-of-sight access, making it unsuitable for curved surfaces.
- Fluid flow mass flow measurements capture mass flow rates through the channel to determine effective flow area. This allows back-calculation of usable flow-through cross-section area using inlet conditions and measured flow rates based on fluid dynamics principles.

RQ3: How does the internal surface roughness of PBF-LB and MBJ injectors affect circumferential uniformity and spray direction under scaled-down engine conditions in a spray rig?

- Smaller AM injector outlets faced significant manufacturing challenges, resulting in increased quality uncertainties and performance variability due to shrinkage and surface roughness, leading to potential need for additional post-processing.

- Larger PBF-LB injector outlets demonstrated better performance in maintaining circumferential spray uniformity and directional stability even if the internal surface roughness is larger than for MBJ injectors.
- The PBF-LB 0.6 mm injector produced a more defined spray core with less break-up and a higher velocity (37 m/s) compared to the MBJ injector (28 m/s). While the spray break-up characteristics between the injectors had little impact on the SMD, droplet size decreased from approximately 125 µm to 104 µm as the distance from the injector outlet increased.

RQ4: How does surface roughness impact the performance of an PBF-LB produced Guide Vane?

- The AM guide vane design and the internal surface roughness of the channels enabled cooling air savings and metal temperature reductions.
- The AM guide vane achieved over 20% cooling air savings and a 56 ºC average reduction in metal temperature and demonstrated more even temperature distributions than the cast counterparts due to flexible internal cooling channel and higher heat transfer designs.
- Surface roughness increased heat transfer efficient with approximately 20%.

8. FUTURE WORK

The recommended future work will primarily focus on efforts within the Tech4H2 competence center, specifically developing AM fuel injectors for combustion with hydrogen-rich fuels. The work can be divided into five different focus areas: fuel injector design, surface roughness, post-processing of internal channels, evaluating new AM methods and spray testing.

- The work presented in this thesis has evaluated only a very simple orifice design. Further research will require the assessment of more advanced fuel injectors, such as atomizers and air-blast injectors.

- The surface roughness measurements of the fuel injectors are not sufficiently detailed and further evaluations are necessary to understand the correlation between spray performance and surface characteristics.

- Potential improvements include refining print strategies and post-processing techniques for smaller injectors to enhance surface quality and circumferential uniformity, with methods such as Hirtization or REM being of particular interest, with input on processing outcome connected to material properties as well.

- Chalmers has recently invested in new LMM printer from Incus. This technique is expected to bring next level of precision in the field of AM. We plan to print set of fuel injectors using LMM technology to evaluate their performance. This requires dedicated process development to bring both printing and sintering in place.

- Further testing is required, including multiple pressure ratios and evaluations of droplet characteristics using Phase Doppler Anemometry (PDA).

9. ACKNOWLEDGEMENTS

I would like to express my gratitude for the support and funding provided by TechForH2, Energimyndigheten and Siemens Energy AB. Their contributions have been instrumental in the success of this project.

I am especially thankful to the team at Siemens Energy AB for their invaluable assistance throughout this project. I would like to especially thank Karl-Johan Nogenmyr, whose unwavering support and generosity have been essential in achieving these results. I would also like to extend big thanks to Daniel Moëll, Daniel Lörstad, Karolina Melki, Mia Gyllenhammar, Vivekanandan Shanmuga Sundaram, Mats Kinell, Magnus Hallberg and many others for your guidance and expertise.

My deep appreciation goes to TechForH2 at Chalmers; Prof. Lars Nyborg, Prof. Yu Cao, Lecturer Mats Norell and Vishnu Anilkumar. Your support and expertise have made this experience very rewarding and I am looking forward to learning more from you. To my colleagues at Chalmers, thank you for making this journey so enjoyable.

I would also like to acknowledge RISE for their assistance with testing and measurements. Special thanks are extended to Marcus Gullberg and Håkan Johansson for your insightful discussions on spray testing and for welcoming me so warmly at RISE Piteå.

To the GARDA group at Chalmers, HANZA, BOMEK, RISE Mölndal and Markforged (formerly Digital Metal), thank you for your efforts in the machining and production of the fuel injectors.

Finally, I want to extend my deepest thanks to my friends, family and partner for their unwavering support throughout this journey.

10. REFERENCES

[1] ASTM/ISO 52900, "Additive Manufacturing - General Principles - Terminology," *ASTM Int.*, vol. 2021, no. II, pp. 1–14, 2021, [Online]. Available: https://www.iso.org/obp/ui/#iso:std:69669:en%0Ahttps://www.iso.org/standard/69669.html%0Ahttps://www.astm.org/Standards/ISOASTM52900.htm

[2] I. Gibson, D. Rosen, B. Stucker, and M. Khorasani, *Additive Manufacturing Technologies*, Third Edit. Cham: Springer, 2021. doi: 10.1007/978-3-031-20752-5_22.

[3] C. Zhang, S. Wang, J. Li, Y. Zhu, T. Peng, and H. Yang, "Additive manufacturing of products with functional fluid channels: A review," *Addit. Manuf.*, vol. 36, no. May, p. 101490, 2020, doi: 10.1016/j.addma.2020.101490.

[4] S. G. Kandlikar and W. J. Grande, "Evolution of microchannel flow passages-thermohydraulic performance and fabrication technology," *Heat Transf. Eng.*, vol. 24, no. 1, pp. 3–17, 2003, doi: 10.1080/01457630304040.

[5] B. Blakey-Milner *et al.*, "Metal additive manufacturing in aerospace: A review," *Mater. Des.*, vol. 209, p. 110008, 2021, doi: 10.1016/j.matdes.2021.110008.

[6] Alex Huckstepp, "Surface Roughness - A Guide To Metal Additive Manufacturing By Digital Alloys - Manufactur3D," 2021. https://manufactur3dmag.com/surface-roughness-a-guide-to-metal-additive-manufacturing-by-digital-alloys/

[7] J. Nikuradse, "Strömungsgesetze in Rauhen Rohren," Berlin, 1933.

[8] K. Huang, J. W. Wan, C. X. Chen, Y. Q. Li, D. F. Mao, and M. Y. Zhang, "Experimental investigation on friction factor in pipes with large roughness," vol. 50, pp. 147–153, 2013, doi: 10.1016/j.expthermflusci.2013.06.002.

[9] H. Schlichting and K. Gersten, *Boundary- Layer Theory*, 9th ed. Berlin: Springer-Verlag Berlin Heidelberg, 2017. doi: 10.1007/978-3-662-52919-5.

[10] A. Triantaphyllou *et al.*, "Surface texture measurement for additive manufacturing," *Surf. Topogr. Metrol. Prop.*, vol. 3, no. 2, 2015, doi: 10.1088/2051-672X/3/2/024002.

[11] M. Ziaee and N. B. Crane, "Binder jetting: A review of process, materials, and methods," *Additive Manufacturing*, vol. 28. Elsevier B.V., pp. 781–801, Aug. 01, 2019. doi: 10.1016/j.addma.2019.05.031.

[12] H. Garg, L. Wang, G. Sahut, and C. Fureby, "Large eddy simulations of fully developed turbulent flows over additively manufactured rough surfaces," *Phys. Fluids*, vol. 35, no. 4, Apr. 2023, doi: 10.1063/5.0143863.

[13] H. Garg, G. Sahut, E. Tuneskog, K. Nogenmyr, and C. Fureby, "Large Eddy Simulations of Flow over Additively Manufactured Surfaces : Impact of Roughness and Skewness on Turbulent Heat Transfer," *Physis of fluids*, pp. 1–16,

2024.

[14] A. J. Wildgoose, K. A. Thole, E. Tuneskog, and L. Wang, “Roughness Related to Cooling Performance of Channels Made Through Additive Manufacturing,” *Turbo Expo Power Land, Sea, Air (Vol. 87011, p. V07BT13A014). Am. Soc. Mech. Eng.*, pp. 1–14, 2023.

[15] A. Vafadar, F. Guzzomi, A. Rassau, and K. Hayward, “Advances in metal additive manufacturing: A review of common processes, industrial applications, and current challenges,” *Appl. Sci.*, vol. 11, no. 3, pp. 1–33, 2021, doi: 10.3390/app11031213.

[16] S. Chowdhury *et al.*, “Laser powder bed fusion: a state-of-the-art review of the technology, materials, properties & defects, and numerical modelling,” *Journal of Materials Research and Technology*, vol. 20. Elsevier Editora Ltda, pp. 2109–2172, Sep. 01, 2022. doi: 10.1016/j.jmrt.2022.07.121.

[17] W. E. Frazier, “Metal additive manufacturing: A review,” *J. Mater. Eng. Perform.*, vol. 23, no. 6, pp. 1917–1928, 2014, doi: 10.1007/s11665-014-0958-z.

[18] T. D. Ngo, A. Kashani, G. Imbalzano, K. T. Q. Nguyen, and D. Hui, “Additive manufacturing (3D printing): A review of materials, methods, applications and challenges,” *Composites Part B: Engineering*, vol. 143. Elsevier Ltd, pp. 172–196, Jun. 15, 2018. doi: 10.1016/j.compositesb.2018.02.012.

[19] H. Fayazfar, J. Sharifi, M. K. Keshavarz, and M. Ansari, *An overview of surface roughness enhancement of additively manufactured metal parts: a path towards removing the post-print bottleneck for complex geometries*, vol. 125, no. 3–4. Springer London, 2023. doi: 10.1007/s00170-023-10814-6.

[20] K. Ljunggren and A. Björnram, “Characterization of Additively Manufactured Surfaces of Cooling Channels,” Linköping University, 2022.

[21] M. Li, W. Du, A. Elwany, Z. Pei, and C. Ma, “Metal binder jetting additive manufacturing: A literature review,” *Journal of Manufacturing Science and Engineering, Transactions of the ASME*, vol. 142, no. 9. American Society of Mechanical Engineers (ASME), Sep. 01, 2020. doi: 10.1115/1.4047430.

[22] S. Sendino, S. Martinez, F. Lartategui, M. Gardon, A. Lamikiz, and J. Jesus, “Effect of powder particle size distribution on the surface finish of components manufactured by laser powder bed fusion,” *Int. J. Adv. Manuf. Technol.*, pp. 789–799, 2023, doi: 10.1007/s00170-022-10423-9.

[23] J. Elambasseril, J. Rogers, C. Wallbrink, D. Munk, M. Leary, and M. Qian, “Laser powder bed fusion additive manufacturing (LPBF-AM): the influence of design features and LPBF variables on surface topography and effect on fatigue properties,” *Crit. Rev. Solid State Mater. Sci.*, vol. 48, no. 1, pp. 132–168, 2023, doi: 10.1080/10408436.2022.2041396.

[24] M. N. Goodhand, K. Walton, L. Blunt, R. J. Miller, and R. Marsden, “The Limitations of Using ‘ R a ’ to Describe Surface Roughness,” vol. 138, no. October 2016, pp. 1–8, 2017, doi: 10.1115/1.4032280.

[25] E. Tuneskog, L. Nyborg, and K.-J. Nogenmyr, “Assessment of surface roughness in additively manufactured channels for fluid applications,” in *Euro PM2024*, 2024.

[26] Y. Bai, G. Wagner, and C. B. Williams, “Effect of particle size distribution on powder packing and sintering in binder jetting additive manufacturing of metals,” *J. Manuf. Sci. Eng. Trans. ASME*, vol. 139, no. 8, pp. 1–6, 2017, doi: 10.1115/1.4036640.

[27] S. Dwivedi, A. R. Dixit, A. K. Das, and A. Nag, “A Novel Additive Texturing of Stainless Steel 316L Through Binder Jetting Additive Manufacturing,” *Int. J. Precis. Eng. Manuf. - Green Technol.*, vol. 10, no. 6, pp. 1605–1613, 2023, doi: 10.1007/s40684-023-00508-5.

[28] A. A. Vu, D. A. Burke, A. Bandyopadhyay, and S. Bose, “Effects of surface area and topography on 3D printed tricalcium phosphate scaffolds for bone grafting applications,” *Addit. Manuf.*, vol. 39, no. December 2020, 2021, doi: 10.1016/j.addma.2021.101870.

[29] E. Tuneskog, K. Nogenmyr, D. Moëll, M. Gullberg, and L. Nyborg, “Exploring Surface Roughness Effects on Spray Performance in Metal Additive Manufactured Fuel Injectors for Gas Turbine Applications,” in *WorldPM2024 Conference Proceedings*, 2024.

[30] A. J. Wildgoose, K. A. Thole, P. Sanders, and L. Wang, “Impact of additive manufacturing on internal cooling channels with varying diameters and build directions,” *J. Turbomach.*, vol. 143, no. 7, Jul. 2021, doi: 10.1115/1.4050336.

[31] M. Kadivar, D. Tormey, and G. McGranaghan, “A review on turbulent flow over rough surfaces: Fundamentals and theories,” *Int. J. Thermofluids*, vol. 10, p. 100077, May 2021, doi: 10.1016/J.IJFT.2021.100077.

[32] C. K. Stimpson, J. C. Snyder, K. A. Thole, and D. Mongillo, “Roughness Effects on Flow and Heat Transfer for Additively Manufactured Channels,” vol. 138, no. May, pp. 1–10, 2016, doi: 10.1115/1.4032167.

[33] A. Nyhlén, M. Kinell, and K. J. Nogenmyr, “Experimental investigation of the thermal performance in additively manufactured mini channels,” *J. Phys. Conf. Ser.*, vol. 2116, no. 1, 2021, doi: 10.1088/1742-6596/2116/1/012032.

[34] A. J. Wildgoose, K. A. Thole, R. Subramanian, L. Kersting, and A. Kulkarni, “Impacts of the Additive Manufacturing Process on the Roughness of Engine Scale Vanes and Cooling Channels,” *J. Turbomach.*, vol. 145, no. 4, Apr. 2023, doi: 10.1115/1.4055973.

[35] C. F. COLEBROOK, “Turbulent Flow in Pipes, with particular reference to the Transition Region between the Smooth and Rough Pipe Laws. (includes plates).,” *J. Inst. Civ. Eng. (London, England)*, vol. 12(8), no. February, pp. 393–422, 1939.

[36] B. Aupoix, “Roughness Corrections for the k – x Shear Stress Transport Model : Status and Proposals,” vol. 137, no. February, pp. 1–10, 2015, doi: 10.1115/1.4028122.

[37] J. P. Bons, “A Review of Surface Roughness Effects in Gas Turbines,” vol. 132, no. April, pp. 1–16, 2010, doi: 10.1115/1.3066315.

[38] C. K. Stimpson, J. C. Snyder, K. A. Thole, and D. Mongillo, “Scaling roughness effects on pressure loss and heat transfer of additively manufactured channels,” *J. Turbomach.*, vol. 139, no. 2, pp. 1–10, 2017, doi: 10.1115/1.4034555.

[39] K. A. Thole, S. P. Lynch, and A. J. Wildgoose, *Review of advances in convective heat transfer developed through additive manufacturing*, 1st ed., vol. 53. Elsevier Inc., 2021. doi: 10.1016/bs.aiht.2021.06.004.

[40] V. D. Molitor, “Experimental Study on Pressure Losses in Additive Manufactured Channels,” RWTH Aachen, 2018.

[41] L. Mazzei, R. Da Soghe, and C. Bianchini, “CALIBRATION OF A CFD METHODOLOGY FOR THE SIMULATION OF ROUGHNESS EFFECTS ON FRICTION AND HEAT TRANSFERIN ADDITIVE MANUFACTURED,” 2021, pp. 1–10.

[42] Y. Zhu *et al.*, “On friction factor of fluid channels fabricated using selective laser melting,” *Virtual Phys. Prototyp.*, vol. 15, no. 4, pp. 496–509, 2020, doi: 10.1080/17452759.2020.1823093.

[43] F. Sanchez, S. Canada, A. Corber, C. Ottawa, B. Mathieu, and C. Siemens, “ASSESSMENT OF SPRAY PARTICLE SIZE ON HOLES CREATED THROUGH ADDITIVE MANUFACTURING METHODS (SLM) VS CONVENTIONALLY DRILLED,” in *Global power and propulsion society*, 2018. [Online]. Available: www.gpps.global

[44] J. C. Snyder and K. A. Thole, “Effect of additive manufacturing process parameters on turbine cooling,” *J. Turbomach.*, vol. 142, no. 5, May 2020, doi: 10.1115/1.4046459.

[45] J. C. Snyder and K. A. Thole, “Tailoring Surface Roughness Using Additive Manufacturing to Improve Internal Cooling,” *J. Turbomach.*, vol. 142, no. 7, Jul. 2020, doi: 10.1115/1.4047380.

[46] M. Lindbäck, K. Frankolin, E. Tuneskog, B. Karlsson, and L. Wang, “DEVELOPMENT AND VALIDATION UNDER ENGINE OPERATION ENVIRONMENT OF ADDTIVELY MANUFACTURED HOT TURBINE PARTS,” in *ASME Turbo Expo 2023*, 2023, pp. 1–10.

[47] C. Zhang, S. Wang, J. Li, Y. Zhu, T. Peng, and H. Yang, “Additive manufacturing of products with functional fluid channels: A review,” *Addit. Manuf.*, vol. 36, Dec. 2020, doi: 10.1016/j.addma.2020.101490.

[48] V. G. McDonell and A. H. Lefebvre, *Atomization and Sprays*, Second edi. Taylor & Francis, CRC Press, 2017.

[49] J. Jedelský *et al.*, “Effect of fabrication method and surface roughness on spray characteristics for small pressure-swirl atomizers,” *J. Manuf. Process.*, vol. 85, no. November 2022, pp. 166–178, 2023, doi: 10.1016/j.jmapro.2022.11.031.

[50] Ramamurthi K and Patnaik R, “UNIFORMITY OF SWIRLED SPRAY FORMED WITH NOZZLES OF VARYING SUREFACE ROUGHNESS,” *At. sprays*, vol. 9, pp. 483–496, 1999.

[51] C. D. Tommila, C. R. Hartsfield, J. J. Redmond, J. R. Komives, and T. E. Shelton, “Performance Impacts of Metal Additive Manufacturing of Very Small Nozzles,” *J. Aerosp. Eng.*, vol. 34, no. 2, pp. 1–11, 2021, doi: 10.1061/(asce)as.1943-5525.0001229.

[52] R. C. Reed, J. J. Moverare, A. Sato, F. Karlsson, and M. Hasselqvist, “A New Single Crystal Superalloy for Power Generation Applications,” *Superalloys 2012*, no. April 2017, pp. 197–204, 2012, doi: 10.1002/9781118516430.ch22.

[53] S. Ritcher, “Surface roughness characterization on additively manufactured Inconel 939 with contact and non-contact measurement instruments,” Linköping University, 2021. [Online]. Available: LIU-IEI-TEK-A-22/04261-SE

[54] M. Risberg, “Spray visualisations of gas-assisted atomisation of black liquor,” Luleå University of Technology, 2008. doi: https://www.diva-portal.org/smash/get/diva2:1015973/FULLTEXT01.pdf.